Biosensors and Bioelectronics 24 (2008) 93–98

Contents lists available at ScienceDirect

Biosensors and Bioelectronics

journal homepage: www.elsevier.com/locate/bios

Porous nanosheet-based ZnO microspheres for the construction of direct electrochemical biosensors

Xianbo Lu, Haijun Zhang, Yuwen Ni, Qing Zhang, Jiping Chen*

Dalian Institute of Chemical Physics, Chinese Academy of Sciences, Dalian 116023, PR China

ARTICLE INFO

Article history:
Received 23 January 2008
Received in revised form 19 March 2008
Accepted 19 March 2008
Available online 1 April 2008

Keywords:
Biosensor
Direct electron transfer
Hydrogen peroxide
Nitrite
ZnO

ABSTRACT

Nanosheet-based ZnO microsphere with porous nanostructures was synthesized by a facile chemical bath deposition method followed by thermal treatment, which was explored for the construction of electrochemical biosensors. Spectroscopic and electrochemical researches revealed the ZnO-based composite was a biocompatible immobilization matrix for enzymes with good enzymatic stability and bioactivity. With advantages of nanostructured inorganic–organic hybrid materials, a pair of stable and well-defined quasi-reversible redox peaks of hemoglobin was obtained with a formal potential of −0.345 V (vs. Ag/AgCl) in pH 7.0 buffer. Facilitated direct electron transfer of the metalloenzymes with an apparent heterogeneous electron transfer rate constant (k_s) of 3.2 s^{-1} was achieved on the ZnO-based enzyme electrode. Comparative studies demonstrated the nanosheet-based ZnO microspheres were more effective in facilitating the electron transfer of immobilized enzyme than solid ZnO microspheres, which may result from the unique nanostructures and larger surface area of the porous ZnO. The prepared biosensor displayed good performance for the detection of H_2O_2 and $NaNO_2$ with a wide linear range of 1–410 and 10–2700 μM, respectively. The entrapped hemoglobin exhibits high peroxidase-like activity for the catalytic reduction of H_2O_2 with an apparent Michaelis-Menten constant (K_M^{app}) of 143 μM. The nanosheet-based ZnO could be a promising matrix for the fabrication of direct electrochemical biosensors, and may find wide potential applications in biomedical detection and environmental analysis.

1. Introduction

The electron transfer between and within proteins is an essential feature for many physiological processes, including biological energy transfer, metabolism and enzymatic catalysis (Bistolas et al., 2005). The use of electrochemistry allows investigating the electrochemical properties of redox enzymes and their mechanism by observing the direct electron transfer in real time. The possibility of direct electron transfer between protein and electrode surface could pave the way for superior reagentless mediator-free biosensing devices, as it obviates the need for co-substrates or mediators and allows efficient transduction of the biorecognition event (Wang, 2005). Since the redox-active center of proteins is deeply embedded in its protein shell, direct electron transfer between the protein and the electrode surface is usually very difficult (Armstrong et al., 1988; Heller, 1990; Scheller et al., 2005; Lu et al., 2006a). On bare electrodes, enzymes tend to denature and to passivate the electrode. Modifying the electrode with an appropriate medium like a polymer, in order to attain native structure and appropriate orientation of the enzyme so increasing electron transfer between the enzyme and the electrode has been very popular in recent years (Bistolas et al., 2005; Huang et al., 2002; Lu et al., 2006b; Wang et al., 2005; Liu et al., 2005).

The fundamental aspects of an electrochemical biosensor involve the enzyme immobilization onto an electrode surface and the formation of efficient electrical communication between the enzyme and the electrode while retaining the enzymatic stability and bioactivity (Zang et al., 2007). To achieve this goal, one promising way is to employ nanostructured materials for the construction of biosensor (Willner et al., 2007; Lu et al., 2007). Owing to their small size and high surface area, nanomaterials have physical, chemical and electronic properties that are different from those of bulk materials. The ability to tailor the size and structure and hence the properties of nanomaterials offers excellent prospects for designing novel sensing systems and enhancing the performance of bioanalytical devices (Wang, 2005; Lin et al., 2004; Moore et al., 2004). Among these nanostructured materials, metal oxide semiconductors are attracting considerable interest in bioanalytical area as they can combine properties of high surface area, non-toxicity, ease of fabrication, optical transparency, chemical stability. As a typical n-type metal oxide semiconductor, ZnO possesses many unique optical and electrical properties for applications in

* Corresponding author. Tel.: +86 411 84379562; fax: +86 411 84379562.
E-mail address: chenjp@dicp.ac.cn (J. Chen).

0956-5663/$ – see front matter © 2008 Elsevier B.V. All rights reserved.
doi:10.1016/j.bios.2008.03.025

many important areas, such as solar cells, chemical sensors, heterogeneous catalysts (Kuo et al., 2005; Wang and Xie, 2006). Many research results revealed that the morphology and structure of nanomaterials have an important effect on its properties, which determines its applications in many fields (Yan and Xue, 2006; Kuo et al., 2005). Here, a nanosheet-based ZnO microsphere with porous nanostructure was synthesized by a simple chemical bath deposition method followed by thermal treatment. There are numerous nanoscaled cavities on the surface of the ZnO microspheres. Both the unique nanostructures and properties of ZnO make it particular promising for applications in biosensors. As a metal oxide semiconductor, nanosheet-based ZnO possesses high surface area, good biocompatibility, optical transparency, chemical and photochemical stability. The numerous nanoscaled cavities on the surface of the microspheres are highly advantageous for the entrapment of enzymes. The porous structure can greatly enhances the active surface area available for protein binding, in which proteins can sequester in the cavities or bind on the surface of the microspheres. Furthermore, the cavities may provide a protective microenvironment for the enzymes to retain their enzymatic stability and activity by limiting the conformational change and unfolding of the entrapped enzymes. Meanwhile, their open frameworks can provide convenience for substrates to access the immobilized enzyme. Up to now, no work has been done using this promising nanomaterial with porous nanostructures for biotechnology applications.

Nafion is a proton-conductive and biocompatible perfluorosulfonate linear polymer that exhibits excellent film-forming ability, which has been used for the immobilization matrix of enzymes (Nadzhafova et al., 2004; Lu et al., 2007). In this work, the porous nanosheet-based ZnO microsphere was combined with Nafion to form a nanostructured inorganic–organic hybrid material, which was explored to fabricate electrochemical biosensor by entrapping heme protein. As a nanostructured inorganic–organic hybrid material, ZnO–Nafion composite could reserve the desirable properties of Nafion and nanostructured ZnO to a large extent. Under the synergetic effect between ZnO and Nafion, facilitated direct electron transfer of hemoglobin has been achieved. In particular, comparative studies revealed that the nanosheet-based porous ZnO microspheres offer significant advantages over solid ZnO microspheres with a smooth surface in facilitating direct electron transfer; the potential impact on the design of bioelectrochemical sensors is significant. The fabricated biosensor was successfully used for the detection of hydrogen peroxide and nitrite, and displayed good performance.

2. Materials and methods

2.1. Materials and apparatus

Hemoglobin (from bovine blood) and Nafion solution (5 wt% in lower aliphatic alcohols) were purchased from Sigma. All other reagents (analytical-grade) were purchased from Tianjin Kermel Chemical Regent Company. All solutions were prepared with Milli-Q water (>18.0 MΩ cm).

Powder X-ray diffraction (XRD) was carried out using a X' Pert PRO (PANalytical, Holland) X-ray Diffractometer with Cu Kα radiation (λ = 1.54178 Å) in the 2θ range of 20–70°. Scanning electron microscope (SEM) images were taken with a scanning electron microscope JSM-6360 (JEOL, Japan) with an accelerating voltage of 24 kV. FTIR spectra were obtained on a PerkinElmer Spectrum GX spectrometer (PerkinElmer Company, USA). Sample films for FTIR spectroscopy were prepared by casting Hb–ZnO–Nafion or Hb solution onto CaF_2 slides and allowed to dry in air. Electrochemical measurements were performed at room temperature using a CHI 440 workstation (CH Instruments, Inc., Austin, USA). The measurements were based on a three-electrode system with the prepared film electrode as the working electrode, a platinum wire as the auxiliary electrode, and an Ag/AgCl (3 M KCl) electrode as the reference electrode. Unless otherwise noted, 50 mM pH 7.0 PBS was used as the electrolyte in all experiments. The buffer solution was purged with highly purified nitrogen for at least 30 min and a nitrogen atmosphere environment was kept in electrochemical measurements.

2.2. Synthesis of nanosheet-based ZnO microsphere

In a typical procedure, an aqueous solution containing 0.05 M zinc nitrate, 0.05 M hexamethylene tetramine, and 0.005 M trisodium citrate was prepared with the help of ultrasonication and stirring. This transparent solution was transferred to a flask and heated at 95 °C in an oil bath for 35 min. Then the flask was removed and cooled to room temperature. The resulting white precipitate was collected and washed several times with deionized water and ethanol before being dried in an oven at 65 °C. Finally, the white precipitate was annealed at 320 °C in air for 1 h to obtain the porous ZnO microspheres.

2.3. Preparation of enzyme electrode

Prior to use, a glassy carbon (GC) electrode with a diameter of 3 mm was polished on a polishing cloth with 1.0, 0.3, 0.05 μm alumina powder respectively and rinsed with deionized water followed by sonicating in acetone, ethanol and deionized water successively. Then, the electrode was dried with purified nitrogen stream. The enzyme electrode was prepared by a simple casting method. Firstly, 2 mg ml^{-1} ZnO suspension was obtained by adding 10 mg of as-prepared porous ZnO into 5 ml water with the aid of ultrasonication and stirring. Then, a suspension (denoted as Suspension I), which finally contained 2.5 mg ml^{-1} Hb, 1 mg ml^{-1} ZnO and 1.25% Nafion, was prepared by mixing appropriate volume of Hb solution (10 mg ml^{-1}, dissolved in 20 mM pH 7.0 PBS), ZnO suspension (2mg ml^{-1}) and Nafion solution (5 wt%) thoroughly. Finally, 4 μl of Suspension I was cast onto the surface of a freshly polished GC electrode to prepare the Hb–ZnO–Nafion/GC electrode. A beaker was covered over the electrode so that water can evaporate slowly in air and a uniform film electrode can be obtained. The dried Hb–ZnO–Nafion/GC electrode was stored at 4 °C in refrigerator when not in use.

For comparison with Hb–ZnO–Nafion/GC, a solid ZnO microsphere with smooth surface (denoted as ZnO(s)) was synthesized and used for the fabrication of Hb–ZnO(s)–Nafion/GC electrodes with similar procedures as described above. Fig. S1 (see Supplementary information) gives the SEM images and XRD patterns of the solid ZnO(s) microspheres with an average diameter of about 1 μm. In control experiment, Hb–Nafion/GC and ZnO–Nafion/GC electrodes were also prepared. The solution containing 2.5 mg ml^{-1} Hb and 1.25% Nafion was used to prepare the Hb–Nafion/GC electrode, and the suspension containing 1.0 mg ml^{-1} ZnO and 1.25% Nafion was used to prepare the ZnO–Nafion/GC electrode. It should be noted that the protein load on the surface of different modified electrodes (except the ZnO–Nafion/GC) was equal. Before electrochemical measurements, all the as-prepared film electrodes were immersed in pH 7.0 PBS for 30 min to remove residual components.

3. Results and discussion

3.1. Characterization of the as-prepared ZnO

Unusual microspheres composed of interconnected sheet-like nanostructures were prepared by a facile chemical bath deposition

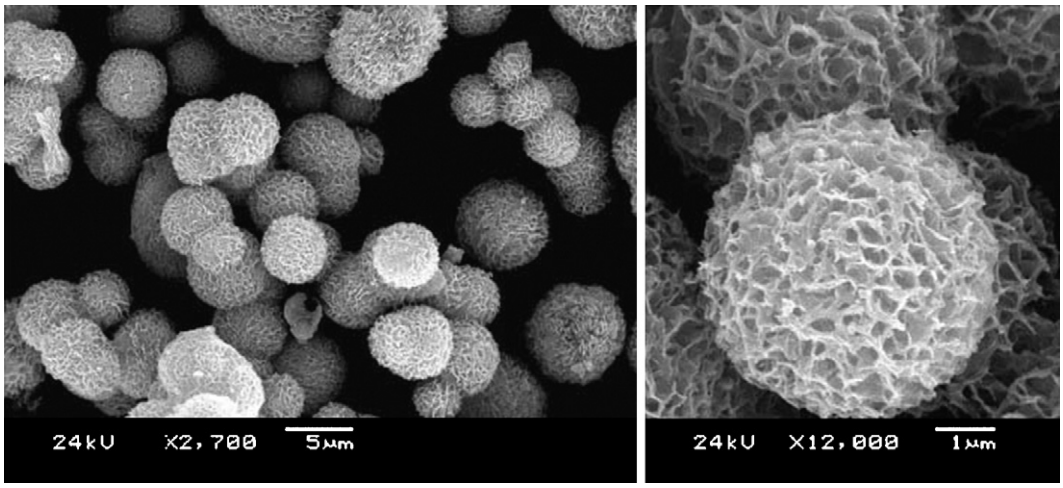

Fig. 1. SEM images of as-prepared porous nanosheet-based ZnO microsphere with low (left) and high magnification (right).

method. Trisodium citrate as a capping regent plays a key role in directing the formation of these microstructures (Kuo et al., 2005; Wang and Xie, 2006). The composition and phase purity of the as-prepared products after thermal treatment were examined by XRD. Fig. S2 (see Supplementary information) shows the XRD patterns of as-prepared ZnO microspheres. It can be seen that all the peaks can be indexed to ZnO with good crystallinity, where no characteristic peaks of impurities appeared.

Fig. 1 shows the SEM images of the as-prepared ZnO microspheres, which are composed of interconnected nanosheets. The thickness of these nanosheets is about 20 nm. The microspheres show a sponge-like pore structure. There are numerous nanoscaled cavities on the surface of the ZnO microspheres. The size of the cavities is about several hundred nanometers, which is accessible for the enzymes to sequester in the cavities or bind on the surface.

3.2. Spectroscopic characterization of Hb–ZnO–Nafion composite film

Hb entrapped in the composite film was firstly investigated by spectroscopic analysis. FTIR spectroscopy is an effective means to probe into the secondary structure of proteins (Wang et al., 2003; Zhou et al., 2002). The characteristic amide I and amide II bands of protein provide detailed information on the secondary structure of polypeptide chain (Kauppinen et al., 1981). The amide I band (1700–1600 cm^{-1}) is attributed to C=O stretching vibration of peptide linkages in the backbone of protein. The amide II band (1620–1500 cm^{-1}) results from the combination of N–H bending and C–N stretching. Nafion presented in spectroscopic characterization contained no polypeptide chain, so it would not interfere with the characterization of amide I and amide II bands of Hb. Fig. 2 shows the in situ FTIR spectra of Hb and Hb–ZnO–Nafion composite film. As shown in Fig. 2a and b, the spectra of amide I and II bands of Hb in Hb–ZnO–Nafion composite film (1658 and 1541 cm^{-1}) are nearly the same as those obtained for native Hb (1658 and 1540 cm^{-1}), and are essentially consistent with the reported value of native Hb (Schlereth and Mlntele, 1992; Lu et al., 2007; Henzler et al., 2007). The similarities of the two spectra suggested that Hb retained the essential features of its native secondary structure in ZnO–Nafion composite film, and revealed the good biocompatibility of ZnO–Nafion composite film. The numerous nanoscaled cavities on the sponge-like surface are highly advantageous for the entrapment of enzymes, in which proteins can sequester in the cavities or bind on the surface of the microspheres. The cavities can provide a protective microenvironment for the enzymes to retain their enzymatic stability and activity by limiting the conformational change and unfolding of the entrapped proteins. The good biocompatibility of the ZnO–Nafion composite can prevent denaturation of the entrapped protein. The ZnO–Nafion composite film provides a promising matrix for enzyme immobilization and biosensor fabrication.

3.3. Direct electron transfer of the enzyme electrode

Fig. 3 shows typical cyclic voltammograms of different modified electrodes in 50 mM pH 7.0 PBS. A pair of stable and well-defined redox peaks of Hb for the $Hb(Fe^{III})/Hb(Fe^{II})$ redox couple transformation, which could be ascribed to the direct electron transfer between the Hb and the underlying electrode, were observed at the Hb–ZnO–Nafion/GC electrode (Fig. 3d). The formal potential $E^{\circ\prime}$ (estimated as $(E_{p,a} + E_{p,c})/2$, where $E_{p,a}$ and $E_{p,c}$ are the anodic and cathodic peak potentials, respectively) of Hb was –0.345 V vs. Ag/AgCl, characteristic of $Hb(Fe^{III/II})$ redox couples in various films (Huang et al., 2002; Wang et al., 2004; Lu et al., 2008). The potential difference ΔE_p between the anodic and cathodic peak potentials, which is directly related to the electron transfer rate, was about 20 mV. Such a small ΔE_p value revealed a fast and quasi-reversible electron-transfer process. There was a pair of negligible redox peaks at about −0.15 V at the ZnO–Nafion/GC electrode (Fig. 3a), which was also observed in other modified electrode

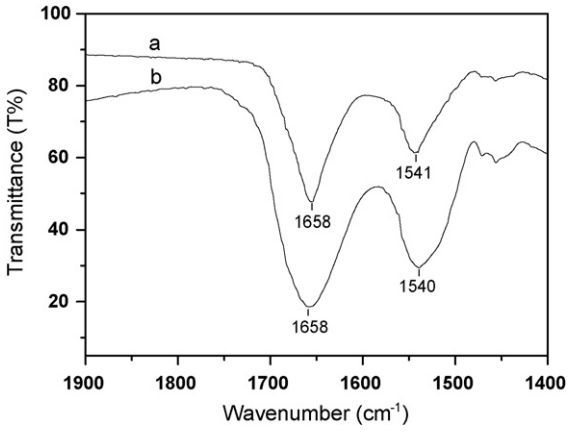

Fig. 2. FTIR of (a) Hb and (b) Hb–ZnO–Nafion composite film.

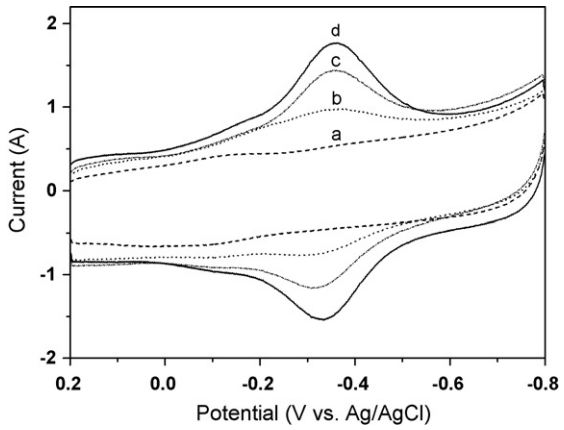

Fig. 3. Cyclic voltammograms of different modified electrode in pH 7.0 PBS with scan rate of 0.2 V s^{-1}: (a) ZnO–Nafion/GC; (b) Hb–Nafion/GC; (c) Hb–ZnO(s)–Nafion/GC; (d) Hb–ZnO–Nafion/GC.

and caused by the electrode matrix Nafion (possibly relevant to the shuttle of H^+ in Nafion). Compared with Hb–ZnO–Nafion/GC electrode, the redox peaks observed at the Hb–Nafion/GC (Fig. 3b) were much smaller. It can be clearly seen from the comparison that direct electron transfer between Hb molecules and GC electrode was greatly enhanced at the Hb–ZnO–Nafion composite film modified electrode. It revealed that ZnO played an important role in facilitating the direct electron transfer of Hb by the synergetic effect with Nafion. The reason that the ZnO–Nafion composite could facilitate the direct electron transfer between the protein molecules and the electrode could be elucidated as follows. Firstly, as we have mentioned, the good biocompatibility of the composite may prevent denaturation and retain the essential secondary structure of the entrapped protein. More importantly, due to its high surface area, the nanosheet-based ZnO can enhance the active surface area of the GC electrode available for protein binding; meanwhile, ZnO may probably act as a rigid framework to favor the appropriate conformation of entrapped proteins, facilitating the direct electron transfer between the redox proteins and the underlying electrode. Moreover, Nafion is a good proton-conducting polymer, the good conductivity of the ZnO–Nafion composite contributes to the efficient electron transfer. Fig. 3c also gives the Cyclic voltammograms of Hb–ZnO(s)–Nafion/GC, which was fabricated with solid ZnO microsphere of about 1 μm diameter with a smooth surface (see Supplementary information, Fig. S1). Compared with Hb–ZnO–Nafion/GC, the redox peaks of Hb–ZnO(s)–Nafion/GC was much smaller. The ΔE_p of Hb–ZnO(s)–Nafion/GC was 40 mV, which was larger than that obtained on Hb–ZnO–Nafion/GC (20 mV), indicating a slower electron transfer rate of Hb on Hb–ZnO(s)–Nafion/GC than on Hb–ZnO–Nafion/GC. By comparison, it can be concluded that porous nanosheet-based ZnO microsphere had better effect on the facilitation of electron transfer than solid ZnO microsphere, which may result from the larger surface area and the porous framework of the nanosheet-based ZnO.

Fig. 4A demonstrates the cyclic voltammograms of Hb–ZnO–Nafion/GC electrode with scan rates from 0.1 to 1.0 V s^{-1}. With the increase of the scan rates, the cathodic and anodic peak currents of Hb increased simultaneously, meanwhile the cathodic and anodic peak potentials showed a small shift and the peak to peak separation also increased. The cathodic and anodic peak currents increased linearly with scan rates from 0.1 to 1.0 V s^{-1}, as shown in Fig. 4B. This revealed that the electron transfer between Hb and GC electrode could be easily performed at the Hb–ZnO–Nafion composite film and it was a surface-controlled electrochemical process. According to the Laviron method for a surface-controlled electrochemical system (Laviron, 1979), the apparent heterogeneous electron transfer rate constant (k_s) of Hb immobilized on Hb–ZnO–Nafion/GC was estimated to be about 3.2 s^{-1}, which was higher than that of Hb immobilized on CNT-based electrode (0.062 s^{-1}) (Zhao et al., 2005) or Co_3O_4-based composite film electrode (2.4 s^{-1}) (Lu et al., 2007), suggesting a faster electron-transfer process. According to Faraday's law, $Q = nFA\Gamma^*$ (where F is Faraday constant, Q can be obtained by integrating the reduction peak of Hb, n and A stand for the number of electron transferred and the geometrical surface area of the electrode, respectively), the surface concentration of electroactive Hb (Γ^*) at Hb–ZnO–Nafion/GC electrode was estimated to be 1.0×10^{-10} mol cm^{-2} (assuming an one-electron transfer reaction). The value obtained in our experiment is about 5 times higher than that of the theoretical monolayer coverage (1.9×10^{-11} mol cm^{-2}) (Wang et al., 2005). This means that multilayers of Hb entrapped in the three-dimensional composite film participated in the electron-transfer process.

3.4. Cyclic voltammetric response of the biosensor for hydrogen peroxide

The determination of H_2O_2 is of great importance in many fields, such as in clinical, food, pharmaceutical and environmental analyses. In bare GC or ZnO–Nafion/GC electrode, there is no obvious electrocatalytic current for H_2O_2 in the potential range from 0.2 to −0.8 V because of the large overpotential of H_2O_2 reduction. The bioelectrocatalytic activity of the enzyme electrode for H_2O_2 is shown in Fig. 5A. When H_2O_2 was added to blank PBS, a significant increase in the cathodic (reduction) peak current was observed

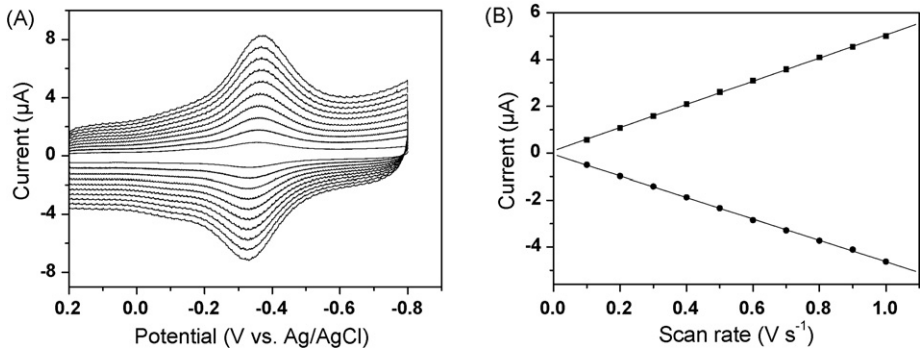

Fig. 4. (A) Cyclic voltammograms of Hb–ZnO–Nafion/GC in pH 7.0 PBS with scan rates from 0.1 to 1.0 V s^{-1}. (B) Plot of cathodic (■) and anodic (●) peak currents vs. scan rates.

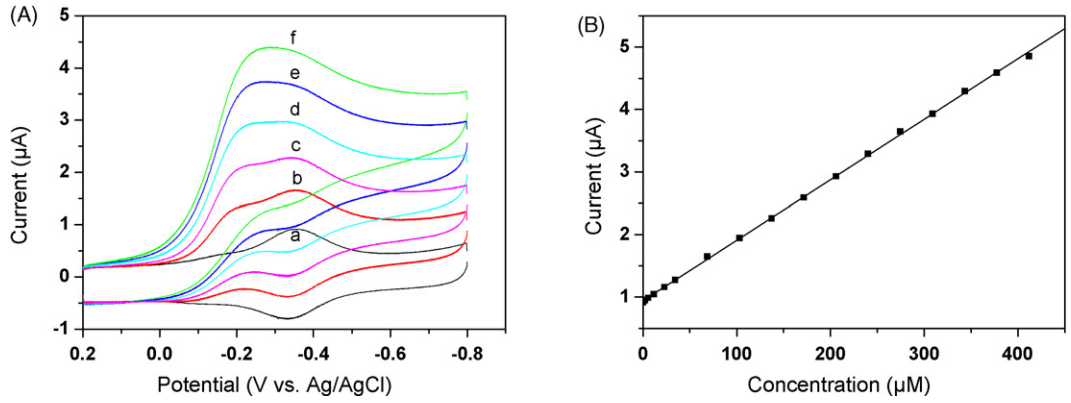

Fig. 5. (A) Bioelectrocatalysis of the biosensor towards H_2O_2 in pH 7.0 PBS with scan rate 0.1 V s^{-1}. H_2O_2 concentrations (μM): (a) 0; (b) 60; (c) 120; (d) 180; (e) 240; (f) 300. (B) The calibration curve of cathodic reduction current vs. H_2O_2 concentration.

accompanying the decrease of anodic (oxidation) peak current, demonstrating a typical electrocatalytic reduction process of H_2O_2 by Hb in the ZnO–Nafion composite. The possible mechanism of electrocatalytic reduction of H_2O_2 at Hb-based enzyme electrode has been reported (Lu et al., 2008; Onuoha et al., 1997; Huang et al., 2002), which can be expressed as follows (Lu et al., 2008):

$$\text{Hb[Heme(Fe}^{\text{III}}\text{)]} + H_2O_2 \rightarrow \text{Compound I} + H_2O \quad (1)$$

$$\text{Compound I} + H_2O_2 \rightarrow \text{Hb[Heme(Fe}^{\text{III}}\text{)]} + H_2O + O_2 \quad (2)$$

$$\text{Hb[Heme(Fe}^{\text{III}}\text{)]} + H^+ + e^- \rightarrow \text{Hb[Heme(Fe}^{\text{II}}\text{)]} \quad \text{at electrode} \quad (3)$$

$$\text{Hb[Heme(Fe}^{\text{II}}\text{)]} + O_2 \rightarrow \text{Hb[Heme(Fe}^{\text{II}}\text{)]-}O_2 \quad \text{fast} \quad (4)$$

$$\text{Hb[Heme(Fe}^{\text{II}}\text{)]-}O_2 + H^+ + e^- \rightarrow \text{Hb[Heme(Fe}^{\text{III}}\text{)]} + H_2O_2 \textit{ at electrode} \quad (5)$$

The overall reaction of (1)–(5) would be:

$$H_2O_2 + 2H^+ + 2e^- \rightarrow 2H_2O \quad (6)$$

So the final product of H_2O_2 and hemoglobin reaction was H_2O. Reactions (1), (2) and (4) can be performed in solution too, and reactions (3) and (5) can be performed on the enzyme electrode. As can be seen from Fig. 5, there are two reduction peaks (around −0.36 and −0.18 V) at lower concentration of H_2O_2. The reduction peak at −0.36 V was consistent with the reduction peak of Hb[Heme(Fe^{III})] at the Hb–ZnO–Nafion/GC electrode, which should correspond to the electrode reaction (3); and the reduction peak at around −0.18 V was consistent with the reduction peak of O_2 at the Hb–ZnO–Nafion/GC electrode, which should correspond to the electrode reaction (5). The addition of H_2O_2 into the buffer accelerated the formation of Hb[Heme(Fe^{III})] and O_2 through reactions (1) and (2), so the reduction peak currents observed at around −0.36 and −0.18 V were all increased with the increasing H_2O_2 concentration, and the latter (−0.18 V) increased faster than the former (−0.36 V), as observed in Fig. 5. When the concentration of H_2O_2 was further increased to a higher concentration, the reduction peak at around −0.36 V was covered (overlapped) by the reduction peak at around −0.18 V, and the two reduction peaks were superposed to one reduction peak. These phenomena mentioned above were also observed in other published papers (Lu et al., 2007, 2008; Wang et al., 2004; Zhou et al., 2005). The cathodic reduction currents at about −0.36 V increased linearly with the increasing H_2O_2 concentration, as shown in Fig. 5B. The linear range was from 1 to 410 μM (R = 0.9998, n = 18), which was much wider than the reported value (Lu et al., 2007; Liu et al., 2004). The sensitivity of the enzyme electrode was as high as 137 mA cm^{-2} M^{-1}, indicating the enzyme electrode had good bioelectrocatalytic activity for H_2O_2. Further increasing the H_2O_2 concentration resulted in a rise in the catalytic current up to a limiting value; such saturation behavior was characteristic of enzyme-based catalysis. The apparent Michaelis-Menten constant (K_M^{app}) was estimated to be 143 μM according to the electrochemical-version of Lineweaver–Burk equation (Kamin and Wilson, 1980). This value was smaller than those ever reported values (Zhao et al., 2005; Liu et al., 2005), indicating that Hb entrapped in the composite film possesses high peroxidase-like activity. Porous nanomaterials provide a larger surface area available for protein binding and decrease the diffusion distance for the substrate to access the immobilized enzyme, which may improve the performance of the enzyme electrode. The selectivity of the biosensor was detected in pH 7.0 PBS by cyclic voltammetry. Tak-

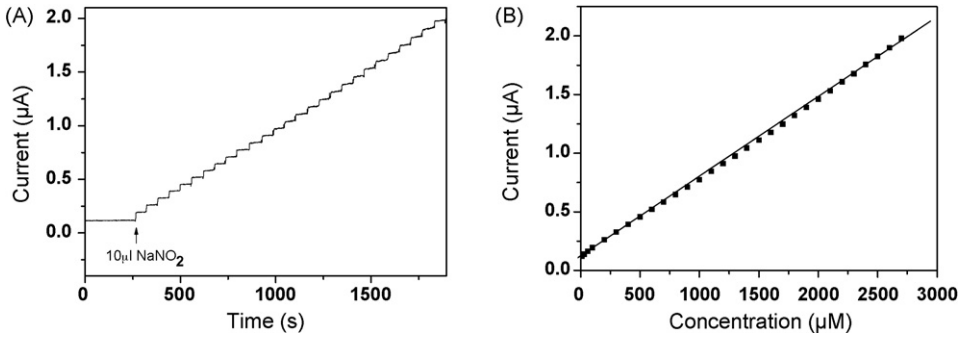

Fig. 6. (A) Typical amperometric current–time response curves of the biosensor upon successive addition of $NaNO_2$ into pH 5.2 acetate buffer solution. Applied potential: −0.675 V (vs. Ag/AgCl). (B) Calibration curve of steady-state currents vs. $NaNO_2$ concentration.

ing sodium nitrite as an example, in the presence of 60 μM (or 120 μM) H_2O_2, the addition of 60 or 120 μM sodium nitrite (final concentration in the supporting electrolyte) did not interfere with the detection of H_2O_2. This is not difficult to understand because the reduction peak of H_2O_2 was at around −0.36 V, while the reduction peak of nitrite was at near −0.8 V (one weak reduction peak in this pH 7.0 buffer). Because of the potential-dependent and pH-dependent characteristics, the fabricated biosensor can detect hydrogen peroxide and nitrite selectively. Other co-existing species such as ascorbic acid, uric acid and glucose (with the same concentration as H_2O_2) did not interfere with the detection of H_2O_2, which might be attributed to the intrinsic selectivity of Hb for its substances and the selectivity of the composite film (especially Nafion) for the negatively charged species in pH 7.0 PBS.

3.5. Amperometric response of the biosensor for nitrite

As is well known, nitrite is a carcinogen that widely exists in antiseptic food and polluted water. It has been reported that Hb-based enzyme electrode has catalytic activity for nitrite, and the possible product at about −0.7 V was N_2O in pH 5.5 buffer (Huang et al., 2002; Lin et al., 1997). The amperometric response of the fabricated biosensor for nitrite was investigated by amperometric current–time curve method. The electrocatalytic reduction peak potential of nitrite at the Hb–ZnO–Nafion/GC in pH 5.2 acetate buffer solution, i.e. −0.675 V, was selected as the constant applied potential for the high sensitivity together with a wide linear range. Fig. 6A demonstrates the typical current–time curve of the biosensor on successive addition of $NaNO_2$. When $NaNO_2$ was added to the stirring buffer, the biosensor responded rapidly to the substrate. The response time (achieving 95% of the steady-state current) was less than 5 s. Such a rapid response can be attributed to the fast diffusion of the substrate in the porous composite film. Fig. 6B shows the typical calibration curve of the steady-state current vs. $NaNO_2$ concentration. As shown, the steady-state response current increased linearly with the increasing $NaNO_2$ concentration. The linear range was very wide, from 10 to 2700 μM, with a correlation coefficient of 0.9997 (n = 30). The detection limit was 4 μM (the signal to noise ratio was 3). The fabricated biosensor can be used repetitively for the detection of nitrite without obvious sensitivity decrease.

3.6. Reproducibility and stability of the biosensor

The reproducibility of the biosensor was investigated at different concentrations in the linear range by cyclic voltammetric measurements. The relative standard deviation (R.S.D.) of the biosensor response to 30 and 120 μM H_2O_2 for 5 successive measurements was 0.48% and 0.8%, respectively, indicating good reproducibility. To evaluate the electrode-to-electrode reproducibility, three biosensors were prepared under the same conditions independently. The R.S.D. of the prepared biosensors was 2%, indicating an acceptable electrode-to-electrode reproducibility.

The biosensor was stored dry or immersed in PBS at 4 °C when it was not in use. The biosensor could retain 96% of its initial response after a 20-day storage, demonstrating good long-term stability. The good long-term stability can be attributed to the good biocompatibility of the composites, which can provide a favorable microenvironment for Hb to retain its bioactivity.

4. Conclusions

Porous nanosheet-based ZnO microspheres were synthesized by a facile chemical bath deposition method followed by thermal treatment. This unique ZnO microsphere with porous nanostructures was explored for the construction of direct electrochemical biosensor and proved to be a good immobilization matrix for proteins and enzymes with good biocompatibility. With advantages of nanostructured inorganic–organic hybrid materials, facilitated direct electron transfer and good bioactivity can be readily achieved by entrapping metalloenzymes into the ZnO-based composite. Comparative studies revealed that the nanosheet-based porous ZnO microspheres offer significant advantages over solid ZnO microspheres in facilitating direct electron transfer; the potential impact on the design of bioelectrochemical sensors is significant. The prepared mediator-free third-generation biosensor displayed good sensitivity and reproducibility, wide linear range, low detection limit, fast response and good long-term stability for the detection of H_2O_2 and $NaNO_2$. The nanosheet-based ZnO proved to be a promising matrix for the fabrication of electrochemical biosensors, and may find wide potential applications in biomedical detection and environmental analysis.

Acknowledgement

This work was financially supported by the National Basic Research Program of China (Grant No. 2003CB415001).

Appendix A. Supplementary data

Supplementary data associated with this article can be found, in the online version, at doi:10.1016/j.bios.2008.03.025.

References

Armstrong, F.A., Hill, H.A.O., Walton, N.J., 1988. Acc. Chem. Res. 21, 407–413.
Bistolas, N., Wollenberger, U., Jung, C., Scheller, F.W., 2005. Biosens. Bioelectron. 20, 2408–2423.
Heller, A., 1990. Acc. Chem. Res. 23, 128–134.
Henzler, K., Wittemann, A., Breininger, E., Ballauff, M., Rosenfeldt, S., 2007. Biomacromolecules 8, 3674–3681.
Huang, H., Hu, N.F., Zeng, Y.H., Zhou, G., 2002. Anal. Biochem. 308, 141–151.
Kamin, R.A., Wilson, G.S., 1980. Anal. Chem. 52, 1198–1205.
Kauppinen, J.K., Moffate, D.J., Mantsch, H.H., Lameron, D.G., 1981. Appl. Spectrosc. 35, 271–276.
Kuo, C.L., Kuo, T.J., Huang, M.H., 2005. J. Phys. Chem. B 109, 20115–20121.
Laviron, E., 1979. J. Electroanal. Chem. 101, 19–28.
Lin, R., Bayachou, M., Greaves, J., Farmer, P.J., 1997. J. Am. Chem. Soc. 119, 12689–12690.
Lin, Y.H., Lu, F., Tu, Y., Ren, Z.F., 2004. Nano Lett. 4, 191–195.
Liu, S.Q., Dai, Z.H., Chen, H.Y., Ju, H.X., 2004. Biosens. Bioelectron. 19, 963–969.
Liu, Z.M., Yang, Y., Wang, H., Liu, Y.L., Shen, G.L., Yu, R.Q., 2005. Sens. Actuators B 106, 394–400.
Lu, X.B., Hu, J.Q., Yao, X., Wang, Z.P., Li, J.H., 2006a. Biomacromolecules 7, 975–980.
Lu, X.B., Wen, Z.H., Li, J.H., 2006b. Biomaterials 27, 5740–5747.
Lu, X.B., Zhou, J.H., Lu, W., Liu, Q., Li, J.H., 2008. Biosens. Bioelectron. 23, 1236–1243.
Lu, X.B., Zou, G.F., Li, J.H., 2007. J. Mater. Chem. 17, 1427–1432.
Moore, R.R., Banks, C.E., Compton, R.G., 2004. Anal. Chem. 76, 2677–2682.
Nadzhafova, O.Y., Zaitsev, V.N., Drozdova, M.V., Vaze, A., Rusling, J.F., 2004. Electrochem. Commun. 6, 205–209.
Onuoha, A.C., Zu, X., Rusling, J.F., 1997. J. Am. Chem. Soc. 119, 3979–3986.
Scheller, F.W., Bistolas, N., Liu, S.Q., Janchen, M., Katterle, M., Wollenberger, U., 2005. Adv. Colloid Interface Sci. 116, 111–120.
Schlereth, D.D., Mlntele, W., 1992. Biochemistry 31, 7494–7502.
Wang, C.H., Yang, C., Song, Y.Y., Gao, W., Xia, X.H., 2005. Adv. Funct. Mater. 15, 1267–1275.
Wang, G., Xu, J.J., Chen, H.Y., Lu, Z.H., 2003. Biosens. Bioelectron. 18, 335–343.
Wang, H., Xie, C., 2006. J. Cryst. Growth 291, 187–195.
Wang, J., 2005. Analyst 130, 421–426.
Wang, Q.L., Lu, G.X., Yang, B.J., 2004. Sens. Actuators B 99, 50–57.
Wang, S.F., Chen, T., Zhang, Z.L., Shen, X.C., Lu, Z.X., Pang, D.W., Wong, K.Y., 2005. Langmuir 21, 9260–9266.
Willner, I., Willner, B., Katz, E., 2007. Bioelectrochemistry 70, 2–11.
Yan, C.L., Xue, D.F., 2006. J. Phys. Chem. B 110, 11076–11080.
Zang, J.F., Li, C.M., Cui, X.Q., Wang, J.X., Sun, X.W., Dong, H., Sun, C.Q., 2007. Electroanalysis 19, 1008–1014.
Zhao, Y.D., Bi, Y.H., Zhang, W.D., Luo, Q.M., 2005. Talanta 65, 489–494.
Zhou, G.J., Wang, G., Xu, J.J., Chen, H.Y., 2002. Sens. Actuators B 81, 334–339.
Zhou, H., Gan, X., Wang, J., Zhu, X.L., Li, G.X., 2005. Anal. Chem. 77, 6102–6104.